iScience

CellPress
OPEN ACCESS

Article

Facile synthesis of water-dispersible poly(3-hexylthiophene) nanoparticles with high yield and excellent colloidal stability

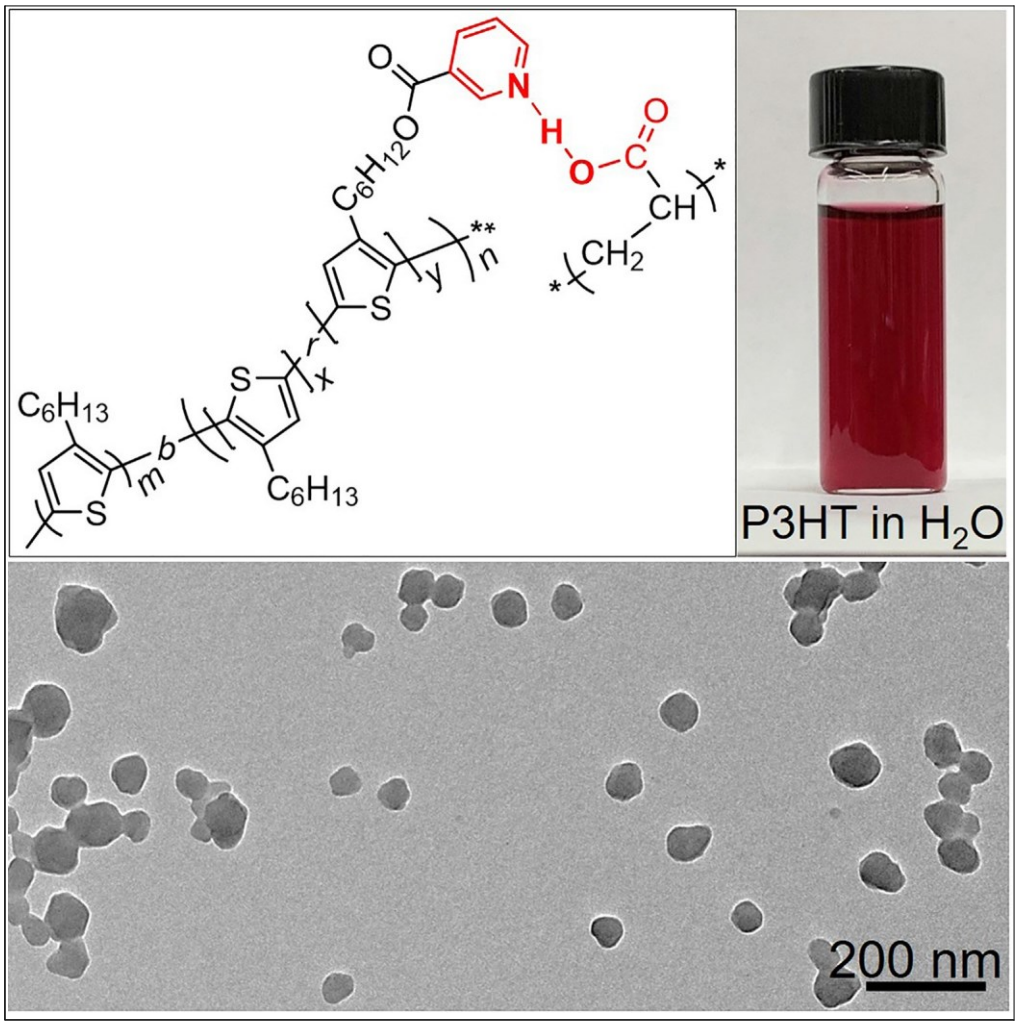

Hanyi Duan, Chao Guan, Jingyi Xue, ..., Yao Lin, Yang Qin, Jie He

yang.qin@uconn.edu (Y.Q.)
jie.he@uconn.edu (J.H.)

Highlights

Water-dispersible P3HT nanoparticles are prepared using nanoprecipitation

P3HT favors H-type aggregates in the presence of PAA

Negatively charged P3HT nanoparticles can bind with metal ions and nanoparticles

Duan et al., iScience 25, 104220
May 20, 2022
https://doi.org/10.1016/j.isci.2022.104220

iScience

CellPress
OPEN ACCESS

Article

Facile synthesis of water-dispersible poly(3-hexylthiophene) nanoparticles with high yield and excellent colloidal stability

Hanyi Duan,[1] Chao Guan,[2] Jingyi Xue,[3] Tessa Malesky,[4] Yangchao Luo,[3] Yao Lin,[1,4] Yang Qin,[1,2,*] and Jie He[1,4,5,*]

SUMMARY

There has been growing interest in water-processable conjugated polymers for biocompatible devices. However, some broadly used conjugated polymers like poly(3-hexylthiophene) (P3HT) are hydrophobic and they cannot be processed in water. We herein report a facile yet highly efficient assembly method to prepare water-dispersible pyridine-containing P3HT (Py-P3HT) nanoparticles (NPs) with a high yield (>80%) and a fine size below 100 nm. It is based on the fast nanoprecipitation of Py-P3HT stabilized by hydrophilic poly(acrylic acid) (PAA). Py-P3HT can form spherical NPs at a concentration up to 0.2 mg/mL with a diameter of rv75 nm at a very low concentration of PAA, e.g., 0.01–0.1 mg/mL, as surface ligands. Those negatively charged Py-P3HT NPs can bind with metal cations and further support the growth of noble metal NPs like Ag and Au. Our self-assembly methodology potentially opens new doors to process and directly use hydrophobic conjugated polymers in a much broader context.

INTRODUCTION

Conjugated polymers (CPs) have received tremendous attention in the past several decades due to their applications in emerging fields including organic field-effect transistors (OFETs) (Kim et al., 2020; Klauk, 2010; Koezuka et al., 1987; Tsumura et al., 1986; Yang et al., 2018), organic photovoltaics (OPVs) (Coakley and McGehee, 2004; Günes et al., 2007; Liu et al., 2016), and organic light-emitting devices (OLEDs) (Boroumand et al., 2005; Greenham et al., 1994; Ho et al., 2000; Liang et al., 2013). The overlapping p-orbitals along CP backbones create delocalized p electrons, resulting in their semiconductive and even conductive as well as tailor-designable optical and electronic properties that are missing in conventional non-conjugated polymers. Poly(3-hexylthiophene) (P3HT) is one of the prototypical and most extensively studied CPs because of its synthetic versatility, solution-processability, attractive electronic properties, and high physical durability. P3HT, therefore, is of broad interest in many applications with extraordinary performance, e.g., as donor materials in OPVs (Lim et al., 2016; Marrocchi et al., 2012), as hole transport materials in perovskite solar cells (Calió et al., 2016), and as p-type semiconductor in OFETs (Sirringhaus, 2014). Because of its hydrophobicity and rigid backbone, P3HT only dissolves in a few non-polar solvents for processing and device fabrication. This largely limits its applications in biocompatible devices, e.g., wearable electronics where organic solvents can be harmful and toxic to human tissues. To this end, water-dispersible polythiophenes have been synthesized with ionic (Brown et al., 2018; Page et al., 2013) or oligo(ethylene oxide) (Lee et al., 2011) side chains. However, these polymers involve alternative synthetic procedures and post-functionalization (Di Maria et al., 2017) that are often time-consuming and cost-ineffective.

To achieve water processability without altering chemical structures of CPs, one possible solution is to form water-dispersible nanoparticles (NPs) through directed self-assembly in solution (Beer et al., 2021; Li et al., 2017; Reichstein et al., 2016; Richards et al., 2011; Subianto et al., 2016; Tan et al., 2016). Those water-dispersible NPs would be streamlined for processing and device fabrication in a more environmentally friendly way. Control of NP size and internal chain packing/aggregate structures also offers additional tools to tune the electronic or optical properties of CPs, as compared to their bulk films (Liu et al., 2009). Because the direct self-assembly approach does not alter the chemical structures of CPs, it preserves the best properties of CPs as originally designed. Water-dispersible P3HT NPs have been extensively explored through two different methods, namely nanoprecipitation (Fraleoni-Morgera et al., 2004; Palamà et al., 2019; Shimizu et al., 2008; Zangoli et al., 2017; Zucchetti et al., 2017) and microemulsion (Nagarjuna et al., 2012).

[1]Polymer Program, Institute of Materials Science, University of Connecticut, Storrs, CT 06269, USA

[2]Chemical & Biomolecular Engineering, University of Connecticut, Storrs, CT 06269, USA

[3]Department of Nutritional Sciences, University of Connecticut, Storrs, CT 06269, USA

[4]Chemistry Department, University of Connecticut, Storrs, CT 06269, USA

[5]Lead contact

*Correspondence: yang.qin@uconn.edu (Y.Q.), jie.he@uconn.edu (J.H.)

https://doi.org/10.1016/j.isci.2022.104220

In nanoprecipitation, P3HT dissolved in a good solvent like tetrahydrofuran (THF) is slowly added to water as a non-solvent for P3HT. The aggregation of collapsed P3HT chains leads to the formation of NPs with a broad-size distribution. Preparation of water-dispersible CP NPs through nanoprecipitation has attracted much attention due to its versatility (e.g., applicable to nearly any conjugated polymers) and accessibility (e.g., without complicated synthetic and purification procedures). As-resultant NPs can be directly used for therapeutics, such as fluorescence/NIR/photoacoustic imaging (Koralli et al., 2020; Luo et al., 2016) and therapeutic agents (Gao et al., 2020; Koralli et al., 2021), and biomedical devices with high biocompatibility (Repenko et al., 2017; Wang et al., 2019). Microemulsion, on the other hand, produces P3HT NPs through oil-in-water emulsion by evaporating organic solvents in the presence of surfactants. Although those NPs can be prepared in a much higher concentration, the size of NPs is usually in the range of a few hundred nanometers. Moreover, the use of surfactants, mostly nonconductive and biocompatible, is detrimental for the device performance and the biomedical applications of those conjugated polymer NPs.

Herein, we report a facile nanoprecipitation method to prepare water-dispersible NPs with a high yield (>80%) and a size below 100 nm. The synthesis is simply based on a ligand-assisted nanoprecipitation with pyridine-containing P3HT (Py-P3HT). Using water-dispersible poly(acrylic acid) (PAA) as ligands, Py-P3HT during solvent exchange can form hydrogen bonding with PAA to stabilize the aggregation of Py-P3HT NPs. The advantage of our method, simply as a combination of nanoprecipitation and stabilizer, is to produce water-dispersible P3HT NPs with high yield, high concentration, high colloidal stability, and surface functionality (e.g., bound with metal cations). In the absence of PAA, nanoprecipitation suffers from a low yield (<2%) of fine particles and the majority of P3HT (>98%) is removed as macroscopic precipitates during purification because hydrophobic P3HT has very weak interaction with water. With the concentration of PAA reaching as low as 0.01 mg/mL, Py-P3HT NPs can assemble into spherical NPs with a diameter of ca. 75 nm as observed by electron microscopy. Those core-shell NPs are water-dispersible with remarkable stability above the pK_a of PAA. The concentration of PAA-capped Py-P3HT NPs can reach as high as 0.2 mg/mL in water without any aggregation after storage for 8 months. The self-assembly method is applicable to prepare Py-P3HT NPs in other organic solvents that are good solvents for PAA but poor solvents for P3HT. Because PAA-capped Py-P3HT NPs are negatively charged, they can bind with metal cations to grow metal NPs on the surface of Py-P3HT NPs. In addition, those surface carboxylic acid groups potentially offer handles to modify the surface chemistry of P3HT NPs, which is of critical importance for their biomedical applications (Mader et al., 2010). We believe this simple method potentially offers many opportunities for easy processing and applications of hydrophobic CPs in aqueous solution.

RESULTS AND DISCUSSION

Py-P3HT was synthesized using quasi-living Grignard metathesis polymerization as previously reported (Li et al., 2013). Briefly, 2-bromo-3-hexyl-5-iodothiophene and ((6-(2-bromo-5-chloromagnesiothiophen-3-yl) hexyl)oxy)(tert-butyl)dimethylsilane were polymerized sequentially with i-PrMgCl as an initiator. After deprotection of silylether moieties, the yielded hydroxyl-functionalized P3HT was further acylated with pyridine. The detailed synthetic procedure of the Py-P3HT was shown in Scheme S1. In the ^{1}H NMR spectra (Figure S1), the peak at 6.98 ppm is assigned to the protons on the thiophene ring and the peak at 2.81 ppm is from the methylene protons that are next to the thiophene moiety. The appearance of the new peak at 3.6 ppm indicates the successful copolymerization with silylether-contaning thiophene monomer. After the hydrolysis and acylation, the representative signal at 9.22, 8.76, 8.26, and 7.36 ppm indicates that P3HT was chemically modified with pyridinyl groups. The molecular weight and dispersity index determined by gel permeation chromatography (GPC) are 46.6 kg/mol and 1.2 (Figure S2), respectively. The ratio of non-functionalized block length to functionalized block length (m/n) is calculated to be 4.5 to 1. The shorter functional block consists of a statistical mixture of 3-hexylthiophene and pyridine-containing hexylthiophene with the ratio of 5/4 (x/y). Thus, the overall pyridine-containing thiophene ratio is about 8% (y/(1 + m/n)) in Py-P3HT.

P3HT NPs were prepared through nanoprecipitation. Py-P3HT was first dissolved into THF at 70°C with a concentration of 0.2 mg/mL. The Py-P3HT solution was then added dropwise through a microsyringe at a rate of 50 mL/min into water with pre-dissolved PAA (1.8 kg/mol from Sigma-Aldrich) under vigorous stirring (1000 rpm). The concentration of PAA was varied to examine its role in nanoprecipitation and the residual THF was evaporated in the fume hood. As a proof-of-concept experiment, Py-P3HT NPs was prepared with 0.05 mg/mL of PAA (Figure 1E) and in the absence of PAA (Figure 1B) under the same conditions. As shown in Figure 1B, the solution of P3HT NPs in the absence of PAA was pinkish.

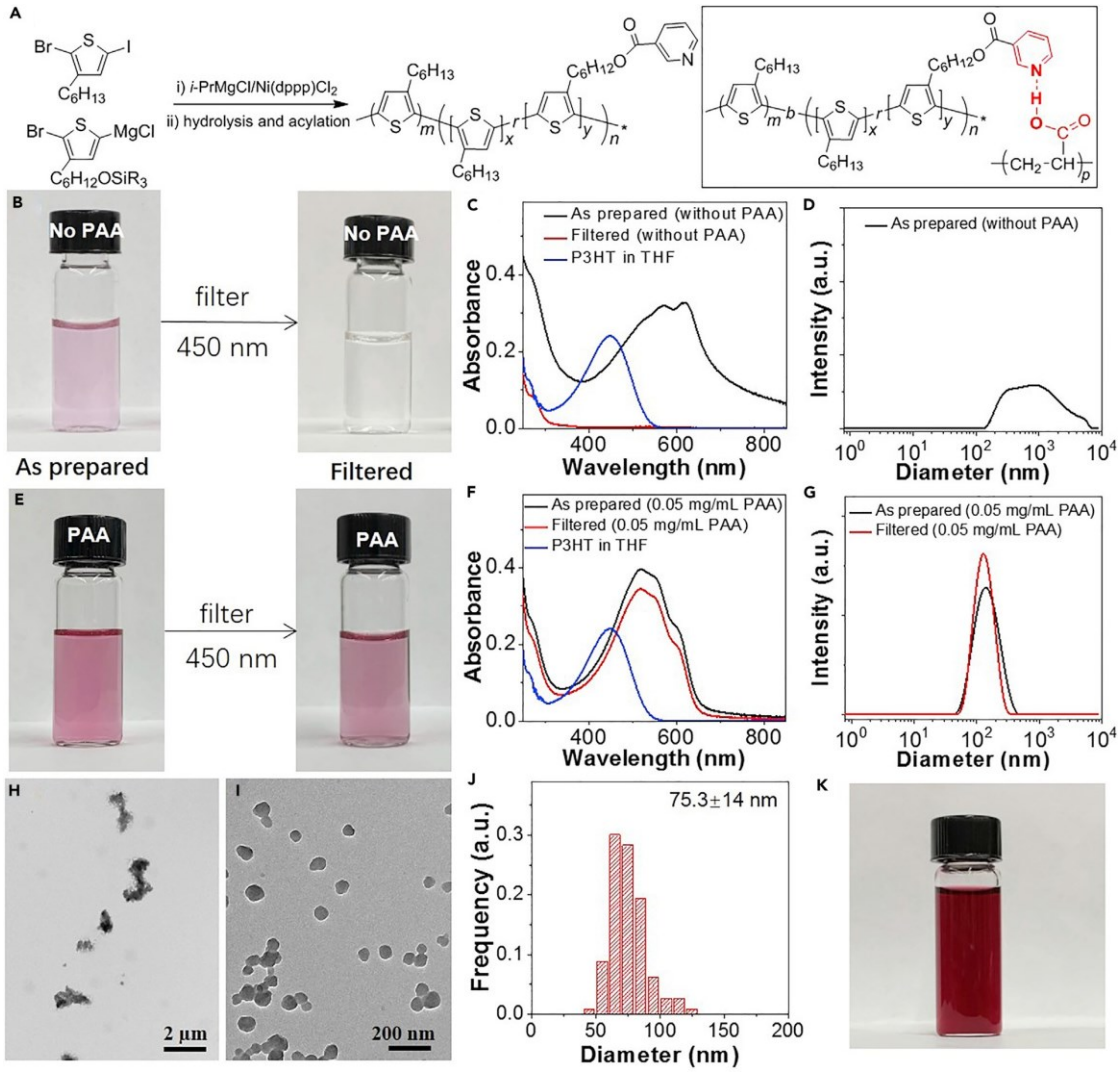

Figure 1. Scheme and characterization of Py-P3HT NPs prepared by PAA-assisted nanoprecipitation

(A) Synthesis and chemical structures of Py-P3HT. The right scheme shows the hydrogen bonding between pyridine units with PAA.

(B) Image, (C) UV-vis and size distribution (D) of Py-P3HT NP solution prepared in the absence of PAA before and after filtration with a 450-nm membrane filter.

(E) Image, (F) UV-vis and (G) size distribution of Py-P3HT NP solution prepared at a PAA concentration of 0.05 mg/mL before and after filtration.

(H and I) TEM images of Py-P3HT NPs prepared without PAA (H) and that with 0.05 mg/mL PAA (I).

(J) Histogram of diameter of P3HT NPs in (I) (Diameter = 75.3 G 14 nm).

(K) Image of the concentrated P3HT NP aqueous solution at 0.1 mg/mL of Py-P3HT after storage for 6 months.

When the solution was passed through a 450-nm membrane filter (polyethersulfone, VWR) to obtain ultrafine Py-P3HT NPs, it became almost colorless (Figure 1B) because large Py-P3HT NPs could not penetrate the filter. In the presence of PAA at a very low concentration of 0.05 mg/mL, the solution of P3HT NPs was red, slightly more concentrated as compared to that in the absence of PAA. After filtered with a 450-nm membrane, there was no apparent change in solution color, indicating that the yield of P3HT NPs was significantly improved. We then used the P3HT absorbance at 521 nm to quantify the yield of Py-P3HT

Table 1. Size and zeta potential of Py-P3HT NPs prepared at various PAA concentrations

	As-prepared			After-filtered		
C_{PAA} (mg/mL)	Diameter (nm)	PDI	z (mV)	Diameter (nm)	PDI	z (mV)
0	619.5	0.418	−26.9	–	–	–
0.01	141.0	0.115	−26.3	135.0	0.131	−27.5
0.05	130.7	0.150	−27.8	122.4	0.089	−26.3
0.1	133.8	0.156	−20.8	125.2	0.085	−21.6
0.5	165.5	0.219	−17.3	130.4	0.067	−22.2
1	158.3	0.117	−15.5	128.2	0.067	−17.2
2	249.3	0.262	−11.2	143.2	0.070	−18.0

NPs (<450 nm), defined as A/A_0 where A_0 and A are the absolute absorbance of P3HT at 521 nm before and after filtration. In the absence of PAA, the yield was less than 2%; that is, >98% of Py-P3HT NPs was removed by the 450-nm filter (Figure 1C). Those results are similar to previously reported examples on nanoprecipitation of conjugated polymers (Shimizu et al., 2008) or hydrophobic organic dyes/chromophores (Frausto and Thomas, 2017, 2018). For Py-P3HT NPs stabilized by PAA, there was only a slight decrease in the absorbance after filtration. The yield of P3HT NPs was 87.1%. This result suggests that Py-P3HT stabilized by PAA formed much smaller, water-dispersible NPs.

The optical properties of Py-P3HT NPs were characterized by UV-vis spectroscopy (Figures 1C, 1F and S3). In THF, the fully dissolved Py-P3HT displays a structureless absorption peak centered at ca. 450 nm. In aggregated states such as thin films and well-defined nanostructures, the absorption profiles of P3HT are red-shifted. In a typical absorption spectrum, shoulder peaks at ca. 605, 550, and 520 nm are typically observed, corresponding to the 0-0, 0-1, and 0-2 vibronic transitions, respectively (Spano, 2006, 2010). The relative intensity between 0-0 and 0-1 transitions is indicative of P3HT solid-state morphologies and crystallinity (Niles et al., 2012; Spano and Silva, 2014). A higher intensity ratio between 0-0 and 0-1 peaks suggests more crystallinity, resulting from intrachain exciton coupling, and thus more planar P3HT chains. In the absence of PAA, the rising 0-0 vibronic transition suggests the increase of intrachain aggregation with more planar P3HT chains that favor J-type aggregates. With PAA, a higher intensity of the 0-1 vibronic transition indicates an H-type-dominated aggregation, resulting from inter-molecular exciton coupling, and thus less planar and more interchain interaction among P3HT chains in the solid state. Those results suggest that PAA interacts with Py-P3HT to vary the chain conformation even faster than the chain pack during solvent exchange. With bound PAA chains, Py-P3HT became less planar with slightly twisted main chains in order to form spherical Py-P3HT NPs with high surface area and curves. Those PAA-capped Py-P3HT NPs had very weak emission in the range 600–800 nm. The lifetime of Py-P3HT NPs is around 0.25 ns in water (Figure S3) measured by time-resolved photoluminescence spectroscopy, similar to the reported values of P3HT NPs (Nagarjuna et al., 2012).

The size of Py-P3HT NPs was firstly examined by dynamic light scattering (DLS). In the absence of PAA, the hydrodynamic diameters (D_H) of Py-P3HT NPs prepared in pure water have a broad distribution of 0.4–2 ㎜ with a polydispersity index (PDI) of 0.49 (Figure 1D). The size of Py-P3HT NPs after filtration cannot be measured due to its low concentration. Note that those Py-P3HT NPs were not stable in solution. The solution color would become colorless after stored for an hour. In contrast, Py-P3HT NPs prepared with 0.05 mg/mL of PAA has an average D_H of 131 nm with a PDI of 0.15. The diameter had a slight decrease to 122 nm after passing the filter. The morphology of Py-P3HT NPs was revealed by transmission electron microscopy (TEM). Without PAA, Py-P3HT segregates have irregular micro-sized shapes with non-spherical surfaces (Figure 1H). With 0.05 mg/mL of PAA, uniform spherical NPs were seen under TEM. The particle size measured from TEM is 75 G 14 nm with its distribution histogram in Figure 1J. The small size difference between TEM and DLS is likely due to the drying.

Py-P3HT NPs with PAA are extremely stable in water. Those NP solutions can be concentrated up to 0.2 mg/mL by vaporing the water. Figure 1K shows a concentrated P3HT NP aqueous solution at 0.1 mg/mL of Py-P3HT after storage for 6 months. No obvious color change and no precipitation were observed. The excellent colloidal stability of Py-P3HT NPs is due to their surface charge. The Zeta potential (z, Table 1)

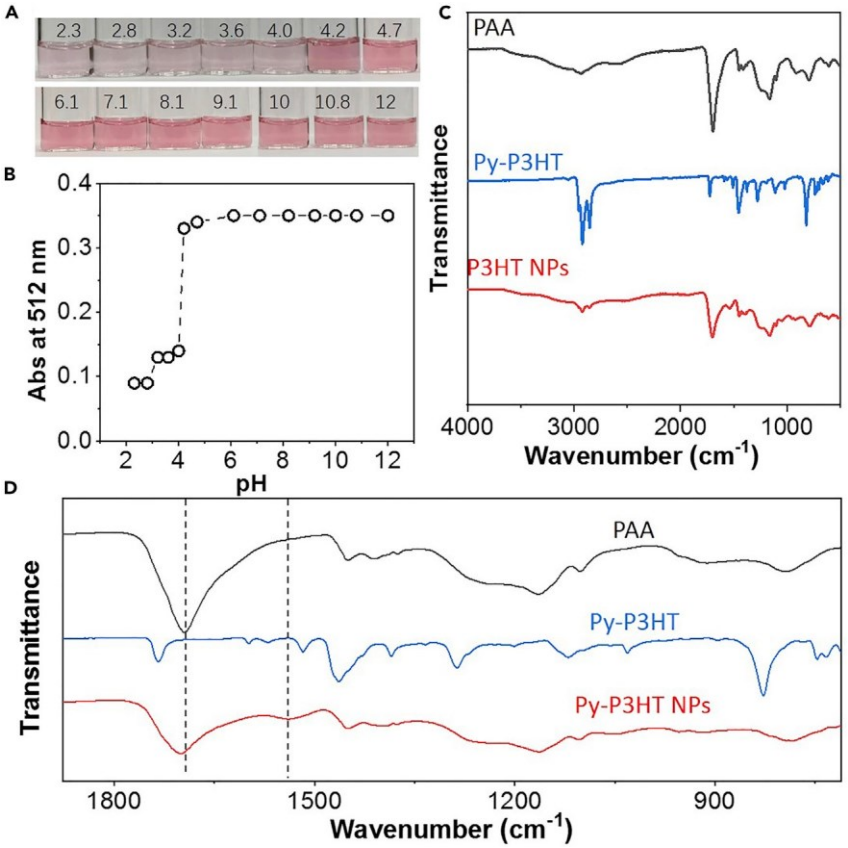

Figure 2. pH titration of Py-P3HT NPs

(A) Images of Py-P3HT NP aqueous solution at various pHs.

(B) Plotting absorbance of Py-P3HT NP solution at 512 nm as a function of pH.

(C and D) FT-IR spectra of PAA, Py-P3HT, and P3HT NP (C) and the zoom-in spectra (D).

of Py-P3HT NPs stabilized by PAA is measured to be −27.8 mV. Because PAA is negatively charged after deprotonation of carboxylic acids, the surface of Py-P3HT NPs is likely capped with PAA to provide electrostatic repulsion and prevent the interparticle collapse of Py-P3HT NPs.

Hydrophobic Py-P3HT, like P3HT, has no solubility in water or polar organic solvents. PAA is, therefore, hypothesized to form as a hydration layer on Py-P3HT NPs, known as surface ligands of hydrophobic Py-P3HT NPs. To confirm whether PAA presents on the surface of Py-P3HT NPs, the stability of Py-P3HT NPs was analyzed through pH titration. Using Py-P3HT NPs prepared at a PAA concentration of 0.05 mg/mL, the solution pH was varied from 12 to 2.3 using HCl and NaOH (1 M). Figure 2A shows the typical images of the Py-P3HT NP solution under various pHs. The NPs were very stable in basic and weakly acidic conditions where no color change was observed in the range of 12 to 4.7. When the pH dropped to 4.2, the solution color became much lighter. There were visible precipitates in the solution as the NPs crushed out. The absorbance change at 512 nm was plotted against pH of the solution as shown in Figure 2B. There was no change in absorbance until the sharp drop occurred at pH 4.2. Because the pK_a of PAA is around 4.5, the change in the NP stability is attributed to the solubility change of PAA. Above its pK_a, the carboxylic acids of PAA are mainly deprotonated where PAA-capped Py-P3HT NPs have strong electronic repulsion. Below its pK_a, the protonation of carboxylic acids results in attraction among Py-P3HT NPs where the collapse of NPs was observed as the solution color diminished.

Fourier transform infrared spectroscopy (FT-IR) was further used to study the interaction between PAA and Py-P3HT. Figure 2C shows the typical FT-IR spectra of PAA, Py-P3HT, and dried PAA-capped Py-P3HT. The peak at 1696 cm^{-1} is assigned to the C=O stretching of carboxylic acids of PAA, while the C=O stretching for the ester groups in Py-P3HT appeared at 1725 cm^{-1}. The broad band above

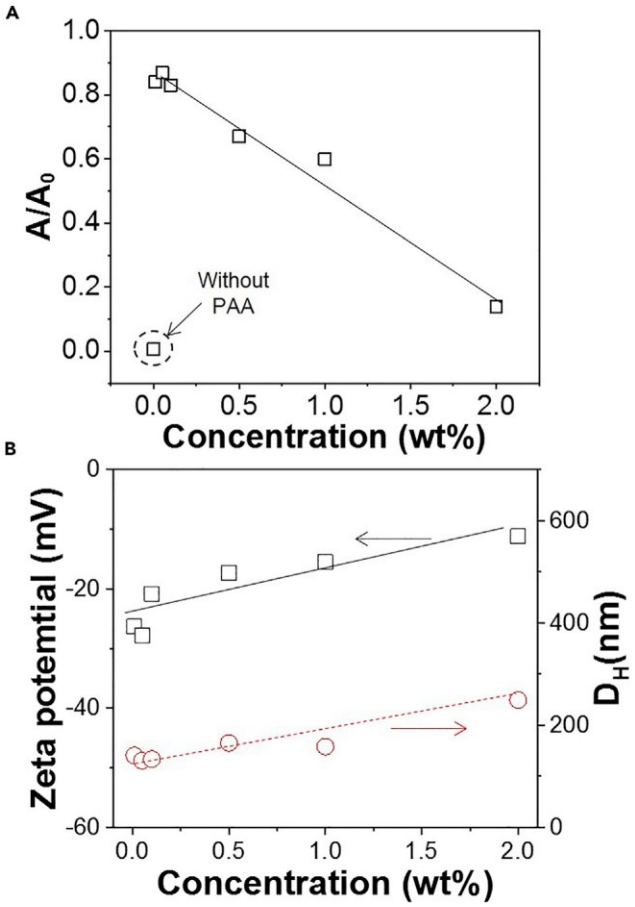

Figure 3. Impact of PAA concentration on Py-P3HT NPs

(A) Yield of Py-P3HT NPs prepared with different concentrations of PAA.

(B) Zeta potential (square) and hydrodynamic diameter (cycle) of Py-P3HT NPs prepared under different concentrations of PAA prior to filtration.

3,000 cm^{-1} is attributed to the O-H stretching of PAA. The peak at 2922 cm^{-1} is assigned the C-H vibration of the hexyl groups in Py-P3HT. The thiophene ring breathing model in Py-P3HT can be identified by the peak at 1460 cm^{-1}. For PAA-capped Py-P3HT, a new vibrational band is seen at 1540 cm^{-1} corresponding to the characteristic peak of pyridine bonded with Brønsted acid (Velthoen et al., 2018; Zhang et al., 2015). Pyridinium-like structures are indicative of hydron-bonded pyridine groups in Py-P3HT. In case of the C=O stretching, there is also a small shift from 1696 cm^{-1} of free PAA to 1700 cm^{-1} of PAA-capped Py-P3HT as often observed in hydrogen-bonded carboxylic acids (Wei et al., 2013). We therefore deduce that PAA stabilizes Py-P3HT as surface ligand through the formation of hydrogen bonding. The multidentate carboxylate groups in PAA would serve as the counter ions to cap the surface of Py-P3HT and thus provide the strong electrostatic repulsion to stabilize hydrophobic Py-P3HT cores. In addition, proton doping from Brønsted acids to P3HT can possibly further stabilize the core-shell NPs, the effect of which is however weak given the absence of absorption signals in the near-IR region typical of doped P3HT (Suh et al., 2020).

While PAA works very effectively to stabilize Py-P3HT NPs even at a very low concentration, the outcome of Py-P3HT NPs, including the yield, size, and surface charge, can be tuned by the concentration of PAA. We first studied the yield of Py-P3HT NPs at various concentrations of PAA in the range of 0.01 mg/mL to 2 mg/mL. Similarly, the UV-vis spectra of Py-P3HT NP solutions before and after filtration were recorded to determine the yield as A/A_0. Those results are summarized in Figure S4. The yield of Py-P3HT NPs shows a linear correlation with the concentration of PAA (Figure 3A). A small amount of PAA, as low as 0.01 mg/mL, was sufficient to stabilize Py-P3HT NPs. The yield of Py-P3HT NPs was in the range of

83%–87% with 0.01 to 0.1 mg/mL of PAA in water. Further increasing the PAA concentration caused a sharp drop in the yield as displayed in in Figure 2A. The yield was down to 67% at 0.5 mg/mL of PAA and it went further down to 14% at 2 mg/mL of PAA. The decrease in the yield of Py-P3HT NPs below 450 nm indicates the size increase of Py-P3HT NPs at a higher concentration of PAA. This presumably is due to the interparticle bridging by PAA where the multiple carboxylic acids can bind with pyridines of different Py-P3HT NPs. The increase of PAA likely decreased the solution pH that also reduced the solubility of those Py-P3HT NPs in solution.

DLS experiments were conducted to measure the D_H of Py-P3HT NPs prepared at different PAA concentrations as plotted in Figure 3B. When PAA concentration increased from 0.01 to 0.1 mg/mL, the D_H of Py-P3HT NPs prior to filtration is around 130.7 nm regardless of PAA concentrations (Table 1 and Figure S5 for DLS results). Those NPs have net negative charges on the surface. The zeta potential of Py-P3HT NPs with 0.05 mg/mL PAA is −27.8 mV. Because those NPs were highly stable in water under natural pHs, the PAA chains were considered to "wrap" around Py-P3HT NPs and bind with pyridines on the surface of individual Py-P3HT NPs. When PAA concentration reached 2 mg/mL, the D_H of NPs increased to 249.3 nm with a broad distribution (Figures S5 and S6). This trend is consistent with the decrease in yield of smaller NPs while large NPs cannot pass the filter. It is, therefore, reasonable to assume that excess PAA promotes interparticle interaction to increase the D_H. The aggregates of NPs also have a lower surface charge, as compared to well-dispersed Py-P3HT NPs prepared with a lower PAA concentration. The zeta potential of Py-P3HT NPs with 2 mg/mL PAA decreased to −11.2 mV. Therefore, the size of Py-P3HT NPs is sensitive to the concentration of PAA. A small amount of PAA is optimal to prepare Py-P3HT NPs with fine sizes and excellent colloidal stability.

Nanoprecipitation assisted by PAA can produce Py-P3HT NPs in a broad range of organic solvents in which PAA has better solubility than Py-P3HT. For example, polar organic solvents like ethanol, methanol and 1,4-dioxane can be used to prepare Py-P3HT NPs. Figure 4A shows the pictures of Py-P3HT NP solution prepared with different solvents with 0.05 mg/mL of PAA. The use of different solvents has a pronounced impact on the solution colors (Figure 4A). The UV-vis spectra of Py-P3HT NPs in different solvents are given in Figure 4C. As compared to Py-P3HT NPs in water, those NPs in organic solvents show less absorption tailed at 520 nm as the 0-2 vibronic transition, closely related to the intraband transition in disordered P3HT chains (Jo et al., 2019). Therefore, in organic solvents, the better solvation allowed P3HT chains (Jo et al., 2019) to pack with increased interchain interaction, although all those NPs display H-type aggregation behaviors. It is noticeable in the absorption spectrum of dioxane solution that there is a small shoulder peak at ca. 450 nm. This is attributed to the presence of fully solvated P3HT chains. TEM images of Py-P3HT NPs prepared in organic solvents are displayed in Figures 4E–4G. Py-P3HT NPs in organic solvents are non-spherical compared with the ones in aqueous solution. All structures seemed to have branched elongated topologies. The size of those irregular NPs is in the range of a few hundred nanometers with a broad distribution. Those structures showed anisotropies as the core crystallinity was improved by organic solvents.

Interestingly, Py-P3HT NPs prepared in dioxane showed right orange emission when excited at 365 nm (Figure 4B), while the fluorescence in other solvents was very weak or less emissive. The emission spectrum of Py-P3HT NPs in dioxane is shown in Figure 4D. A sharp emission peak centered at 575 nm along with a shoulder peak at 608 nm was seen. The emission is likely from the solvated Py-P3HT chains because of their much higher fluorescence intensity. These solvated P3HT chains are likely located on the peripheries of NPs where the localized concentration of PAA is high. In the absence of PAA, Py-P3HT is not emissive in dioxane.

Because Py-P3HT NPs are capped with PAA, those fluorescent NPs in dioxane can interact with transition metal cations, e.g., as fluorescent probes to measure heavy metal ions. As a proof of concept, we examined the fluorescence quenching of Py-P3HT NPs by Cu^{2+} ions. In dioxane with 0.01 mg/mL of Py-P3HT NPs, the fluorescence titration was carried out by adding $CuCl_2$ aqueous solution (Figure 5). Cu^{2+} ions that bind with negatively charged Py-P3HT NPs can quench the fluorescence of Py-P3HT NPs. With 40 mL of 100 mM $CuCl_2$, about 80% of emission of Py-P3HT NPs was quenched. Other transition metal ions, like Co^{2+}, can quench the fluorescence of Py-P3HT NPs as well (Figure S7) since metal ions interact with PAA-capped Py-P3HT NPs through non-specific electrostatic interactions. In addition, those water-dispersible Py-P3HT NPs can further be used to grow metal NPs. As a p-type semiconductor, photoexcited electrons

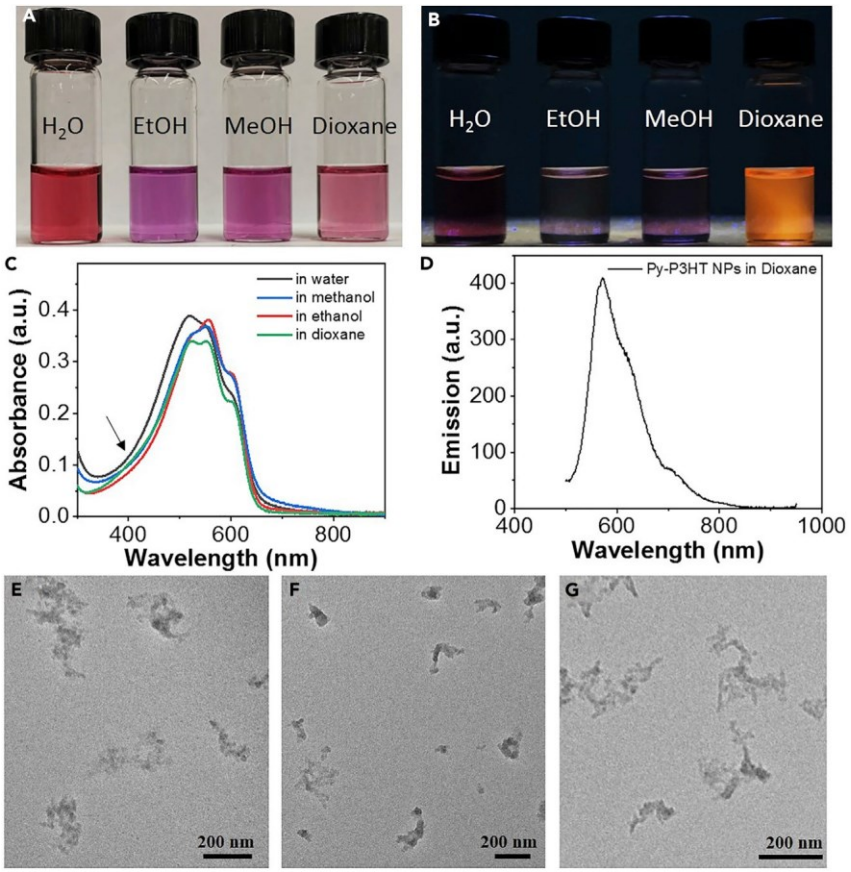

Figure 4. Solvent effect on Py-P3HT NPs

(A and B) Images of Py-P3HT NP solution prepared with different precipitants under sunlight (A) and 365-nm irradiation (B).

(C) UV-vis absorption spectra of Py-P3HT NPs in different solvents.

(D) Emission spectra of Py-P3HT NPs prepared in dioxane.

(E–G) TEM images of Py-P3HT NPs prepared in ethanol (E), methanol (F), and dioxane (G).

of Py-P3HT are highly reductive to generate metal NPs in situ (see supplemental information for details). When excited by visible light (>400 nm), noble metal NPs like Ag and Au with a diameter of a few to tens of nanometers can grow on the surface of Py-P3HT NPs that likely will be of interest for photocatalysis and photovoltaics (Figure S8) (Pan et al., 2016). In addition, it is reasonable to assume that the surface PAA chains can possibly interact with other materials, e.g., fullerene derivatives, to improve the interfaces for photovoltaic device applications (Tang et al., 2011; Tokuhisa and Hammond, 2003).

Conclusion

In summary, we demonstrated a facile but highly efficient method to prepare water-dispersible P3HT NPs with >80% yield. The synthesis was simply based on PAA-assisted nanoprecipitation where water-dispersible PAA interacted with Py-P3HT during solvent exchange and stabilized Py-P3HT NPs. With a very low concentration range of PAA, e.g., 0.01–0.1 mg/mL, sub 100 nm Py-P3HT NPs could be prepared in water with high yield and excellent colloidal stability. PAA-capped Py-P3HT NPs could reach 0.2 mg/mL in water without any aggregation. In the presence of PAA, we found that Py-P3HT NPs favored H-type aggregates where P3HT chains bound with PAA were slightly twisted for interchain interaction. While PAA acted as the surface ligands to stabilize Py-P3HT NPs, excess PAA would result in interparticle aggregation by bridging those surface pyridines among multiple NPs. This methodology was applicable to prepare Py-P3HT NPs directly in other organic solvents as well. Negatively charged Py-P3HT NPs were able to bind with metal cations and further support the growth of metal NPs. Our results could potentially offer new opportunities

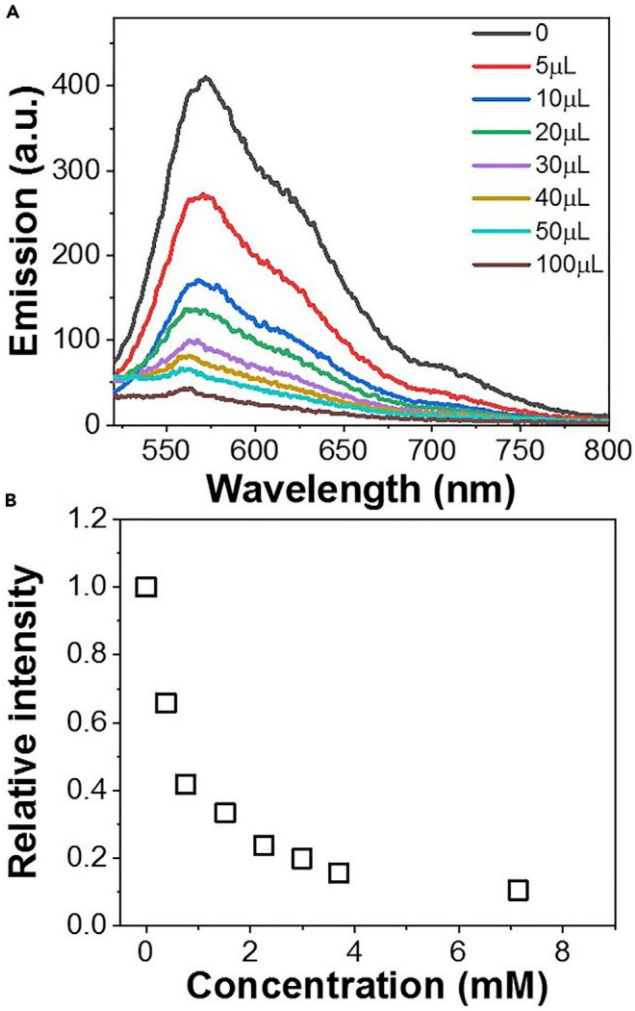

Figure 5. Fluorescence quenching

(A) Emission spectra of Py-P3HT NPs in dioxane with different amount of copper chloride solution (100 mM).

(B) Plotting emission intensity at the maximum emission peak against copper concentration.

in utilizing hydrophobic conjugated polymers in a broad range of applications such as nanomedicine, photocatalysis, and organic electronics.

Limitations of the study

In this work, a facile yet highly efficient method to prepare water-dispersible P3HT NPs was developed with a high yield and controllable size. As-prepared P3HT NPs exhibited excellent colloidal stability and distinctive optical properties. However, currently, the applications of those water-soluble P3HT NPs for photocatalysis are limited by the solvent shifting, which is probably due to their unique surface chemistry. The future work will focus on expanding the conjugated polymer scope and optimizing the condition of the P3HT NPs-metal NPs as hybrid catalysts in photocatalysis.

STAR+METHODS

Detailed methods are provided in the online version of this paper and include the following:

- KEY RESOURCES TABLE
- RESOURCE AVAILABILITY
  - Lead contact

SUPPLEMENTAL INFORMATION

Supplemental information can be found online at https://doi.org/10.1016/j.isci.2022.104220.

ACKNOWLEDGMENTS

Y.Q. thanks the National Science Foundation (CHE-2101535) for the partial support of this work. J.H. is grateful for the continuous financial support from the University of Connecticut, the Green Emulsions, Micelles and Surfactants (GEMS) Center, and the National Science Foundation (CBET-2102245). The TEM studies were performed using the facilities in the Bioscience Electron Microscopy Laboratory at the University of Connecticut (UConn).

AUTHOR CONTRIBUTIONS

J.H., Y.Q., Y.L., and H.D. conceived the research idea. H.D., C.G., J.X., and T.M. performed the experiments, and analyzed the data. C.G. did the synthesis of polymer. H.D. did the preparation and characterization of nanoparticles. Z.X. and Y.C.L. helped to collect and analyze the DLS and zeta potential data. The manuscript was drafted by H.D. and J.H. and all co-authors have contributed to revise and finalize the manuscript.

DECLARATION OF INTERESTS

The authors declare no competing interests.

Received: December 13, 2021
Revised: March 8, 2022
Accepted: April 4, 2022
Published: May 20, 2022

REFERENCES

Beer, P., Reichstein, P.M., Schötz, K., Raithel, D., Thelakkat, M., Köhler, J., Panzer, F., and Hildner, R. (2021). Disorder in P3HT nanoparticles probed by optical spectroscopy on P3HT-b-PEG micelles. J. Phys. Chem. A 125, 10165–10173. https://doi.org/10.1021/acs.jpca.1c08377.

Boroumand, F.A., Fry, P.W., and Lidzey, D.G. (2005). Nanoscale conjugated-polymer light-emitting diodes. Nano Lett. 5, 67–71.

Brown, D.M., Yang, J., Strach, E.W., Khalil, M.I., and Whitten, D.G. (2018). Size and substitution effect on antimicrobial activity of polythiophene polyelectrolyte derivatives under photolysis and dark conditions. Photochem. Photobiol. 94, 1116–1123. https://doi.org/10.1111/php.13013.

Calio, L., Kazim, S., Grätzel, M., and Ahmad, S. (2016). Hole-transport materials for perovskite solar cells. Angew. Chem. Int. Ed. 55, 14522–14545.

Coakley, K.M., and McGehee, M.D. (2004). Conjugated polymer photovoltaic cells. Chem. Mater. 16, 4533–4542.

Di Maria, F., Zanelli, A., Liscio, A., Kovtun, A., Salatelli, E., Mazzaro, R., Morandi, V., Bergamini, G., Shaffer, A., and Rozen, S. (2017). Poly (3-hexylthiophene) nanoparticles containing thiophene-s, s-dioxide: tuning of dimensions, optical and redox properties, and charge separation under illumination. ACS Nano 11, 1991–1999.

Fraleoni-Morgera, A., Marazzita, S., Frascaro, D., and Setti, L. (2004). Influence of a non-ionic surfactant on the UV–vis absorption features of regioregular head-to-tail poly(3-hexylthiophene) in water-based dispersions. Synth. Met. 147, 149–154. https://doi.org/10.1016/j.synthmet.2004.06.039.

Frausto, F., and Thomas, S.W. (2017). Ratiometric singlet oxygen detection in water using acene-doped conjugated polymer nanoparticles. ACS Appl. Mater. Interfaces 9, 15768–15775. https://doi.org/10.1021/acsami.7b02034.

Frausto, F., and Thomas, S.W., III (2018). Tuning the key properties of singlet oxygen-responsive acene-doped conjugated polymer nanoparticles. ChemPhotoChem 2, 632–639.

Gao, D., Hu, D., Liu, X., Zhang, X., Yuan, Z., Sheng, Z., and Zheng, H. (2020). Recent advances in conjugated polymer nanoparticles for NIR-II imaging and therapy. ACS Appl. Mater. Interfaces 2, 4241–4257.

Greenham, N.C., Friend, R.H., and Bradley, D.D. (1994). Angular dependence of the emission from a conjugated polymer light-emitting diode: implications for efficiency calculations. Adv. Mater. 6, 491–494.

Günes, S., Neugebauer, H., and Sariciftci, N.S. (2007). Conjugated polymer-based organic solar cells. Chem. Rev. 107, 1324–1338.

Ho, P.K., Kim, J.-S., Burroughes, J.H., Becker, H., Li, S.F., Brown, T.M., Cacialli, F., and Friend, R.H. (2000). Molecular-scale interface engineering for polymer light-emitting diodes. Nature 404, 481–484.

Jo, G., Jung, J., and Chang, M. (2019). Controlled self-assembly of conjugated polymers via a solvent vapor pre-treatment for use in organic field-effect transistors. Polymers 11, 332.

Kim, M., Ryu, S.U., Park, S.A., Choi, K., Kim, T., Chung, D., and Park, T. (2020). Donor–acceptor-conjugated polymer for high-performance organic field-effect transistors: a progress report. Adv. Funct. Mater. 30, 1904545.

Klauk, H. (2010). Organic thin-film transistors. Chem. Soc. Rev. 39, 2643–2666.

Koezuka, H., Tsumura, A., and Ando, T. (1987). Field-effect transistor with polythiophene thin film. Synth. Met. 18, 699–704.

Koralli, P., Nega, A.D., Vagiaki, L.E., Pavlou, A., Siskos, M.G., Dimitrakopoulou-Strauss, A., Gregoriou, V.G., and Chochos, C.L. (2020). New conjugated polymer nanoparticles with high photoluminescence quantum yields for far-red and near infrared fluorescence bioimaging. Mater. Chem. Front. 4, 2357–2369.

Koralli, P., Tsikalakis, S., Goulielmaki, M., Arelaki, S., Müller, J., Nega, A.D., Herbst, F., Ball, C.R., Gregoriou, V.G., and Dimitrakopoulou-Strauss, A. (2021). Rational design of aqueous conjugated polymer nanoparticles as potential theranostic agents of breast cancer. Mater. Chem. Front. 5, 4950–4962.

Lee, E., Hammer, B., Kim, J.-K., Page, Z., Emrick, T., and Hayward, R.C. (2011). Hierarchical helical assembly of conjugated poly(3-hexylthiophene)-block-poly(3-triethylene glycol thiophene) diblock copolymers. J. Am. Chem. Soc. 133, 10390–10393. https://doi.org/10.1021/ja2038547.

Li, F., Yang, J., and Qin, Y. (2013). Synthesis and characterization of polythiophene block copolymer and fullerene derivative capable of "three-point" complementary hydrogen bonding interactions and their application in bulk-heterojunction solar cells. J. Polym. Sci. A. Polym. Chem. 51, 3339–3350. https://doi.org/10.1002/pola.26731.

Li, J.-H., Li, Y., Xu, J.-T., and Luscombe, C.K. (2017). Self-assembled amphiphilic block copolymers/CdTe nanocrystals for efficient aqueous-processed hybrid solar cells. ACS Appl. Mater. Interfaces 9, 17942–17948. https://doi.org/10.1021/acsami.7b03074.

Liang, J., Li, L., Niu, X., Yu, Z., and Pei, Q. (2013). Elastomeric polymer light-emitting devices and displays. Nat. Photon. 7, 817–824.

Lim, E.L., Yap, C.C., Teridi, M.A.M., Teh, C.H., and Jumali, M.H.H. (2016). A review of recent plasmonic nanoparticles incorporated P3HT:PCBM organic thin film solar cells. Org. Electron. 36, 12–28.

Liu, J., Arif, M., Zou, J., Khondaker, S.I., and Zhai, L. (2009). Controlling poly(3-hexylthiophene) crystal dimension: nanowhiskers and nanoribbons. Macromolecules 42, 9390–9393. https://doi.org/10.1021/ma901955c.

Liu, C., Wang, K., Gong, X., and Heeger, A.J. (2016). Low bandgap semiconducting polymers for polymeric photovoltaics. Chem. Soc. Rev. 45, 4825–4846. https://doi.org/10.1039/C5CS00650C.

Luo, W., Wu, M., Li, S., Xu, Y., Ye, Z., Wei, L., Chen, B., Xu, Q.-H., and Xiao, L. (2016). Nanoprecipitation of fluorescent conjugated polymer onto the surface of plasmonic nanoparticle for fluorescence/dark-field dual-modality single particle imaging. Anal. Chem. 88, 6827–6835.

Mader, H.S., Kele, P., Saleh, S.M., and Wolfbeis, O.S. (2010). Upconverting luminescent nanoparticles for use in bioconjugation and bioimaging. Curr. Opin. Chem. Biol. 14, 582–596.

Marrocchi, A., Lanari, D., Facchetti, A., and Vaccaro, L. (2012). Poly (3-hexylthiophene): synthetic methodologies and properties in bulk heterojunction solar cells. Energy Environ. Sci. 5, 8457–8474.

Nagarjuna, G., Baghgar, M., Labastide, J.A., Algaier, D.D., Barnes, M.D., and Venkataraman, D. (2012). Tuning aggregation of poly (3-hexylthiophene) within nanoparticles. ACS Nano 6, 10750–10758.

Niles, E.T., Roehling, J.D., Yamagata, H., Wise, A.J., Spano, F.C., Moulé, A.J., and Grey, J.K. (2012). J-aggregate behavior in poly-3-hexylthiophene nanofibers. J. Phys. Chem. Lett. 3, 259–263.

Page, Z.A., Duzhko, V.V., and Emrick, T. (2013). Conjugated thiophene-containing polymer zwitterions: direct synthesis and thin film electronic properties. Macromolecules 46, 344–351. https://doi.org/10.1021/ma302232q.

Palamà, I.E., Di Maria, F., Zangoli, M., D'Amone, S., Manfredi, G., Barsotti, J., Lanzani, G., Ortolani, L., Salatelli, E., and Gigli, G. (2019). Enantiopure polythiophene nanoparticles. Chirality dependence of cellular uptake, intracellular distribution and antimicrobial activity. RSC Adv. 9, 23036–23044.

Pan, S., He, L., Peng, J., Qiu, F., and Lin, Z. (2016). Chemical-bonding-directed hierarchical assembly of nanoribbon-shaped nanocomposites of gold nanorods and poly (3-hexylthiophene). Angew. Chem. Int. Ed. 128, 8828–8832.

Reichstein, P.M., Gödrich, S., Papastavrou, G., and Thelakkat, M. (2016). Influence of composition of amphiphilic double-crystalline P3HT-b-PEG block copolymers on structure formation in aqueous solution. Macromolecules 49, 5484–5493. https://doi.org/10.1021/acs.macromol.6b01305.

Repenko, T., Rix, A., Ludwanowski, S., Go, D., Kiessling, F., Lederle, W., and Kuehne, A.J. (2017). Bio-degradable highly fluorescent conjugated polymer nanoparticles for bio-medical imaging applications. Nat. Commun. 8, 1–8.

Richards, J.J., Weigandt, K.M., and Pozzo, D.C. (2011). Aqueous dispersions of colloidal poly(3-hexylthiophene) gel particles with high internal porosity. J. Colloid Interface Sci. 364, 341–350. https://doi.org/10.1016/j.jcis.2011.08.037.

Shimizu, H., Yamada, M., Wada, R., and Okabe, M. (2008). Preparation and characterization of water self-dispersible poly (3-hexylthiophene) particles. Polym. J. 40, 33–36.

Sirringhaus, H. (2014). 25th anniversary article: organic field-effect transistors: the path beyond amorphous silicon. Adv. Mater. 26, 1319–1335.

Spano, F.C. (2006). Absorption in regio-regular poly (3-hexyl) thiophene thin films: fermi resonances, interband coupling and disorder. Chem. Phys. 325, 22–35.

Spano, F.C. (2010). The spectral signatures of Frenkel polarons in H-and J-aggregates. Acc. Chem. Res. 43, 429–439.

Spano, F.C., and Silva, C. (2014). H-and J-aggregate behavior in polymeric semiconductors. Annu. Rev. Phys. Chem. 65, 477–500.

Subianto, S., Dutta, N., Andersson, M., and Choudhury, N.R. (2016). Bulk heterojunction organic photovoltaics from water-processable nanomaterials and their facile fabrication approaches. Adv. Colloid Interface Sci. 235, 56–69. https://doi.org/10.1016/j.cis.2016.05.013.

Suh, E.H., Oh, J.G., Jung, J., Noh, S.H., Lee, T.S., and Jang, J. (2020). Brønsted acid doping of P3HT with largely soluble tris (pentafluorophenyl) borane for highly conductive and stable organic thermoelectrics via one-step solution mixing. Adv. Energy Mater. 10, 2002521.

Tan, B., Li, Y., Palacios, M.F., Therrien, J., and Sobkowicz, M.J. (2016). Effect of surfactant conjugation on structure and properties of poly(3-hexylthiophene) colloids and field effect transistors. Colloids Surf. A. Physicochem. Eng. Asp. 488, 7–14. https://doi.org/10.1016/j.colsurfa.2015.10.002.

Tang, Z., Liu, Q., Tang, Q., Wu, J., Wang, J., Chen, S., Cheng, C., Yu, H., Lan, Z., Lin, J., and Huang, M. (2011). Preparation of PAA-g-CTAB/PANI polymer based gel-electrolyte and the application in quasi-solid-state dye-sensitized solar cells. Electrochim. Acta 58, 52–57. https://doi.org/10.1016/j.electacta.2011.08.074.

Tokuhisa, H., and Hammond, P.T. (2003). Solid-state photovoltaic thin films using TiO2, organic dyes, and layer-by-layer polyelectrolyte nanocomposites. Adv. Funct. Mater. 13,

831–839. https://doi.org/10.1002/adfm.200304404.

Tsumura, A., Koezuka, H., and Ando, T. (1986). Macromolecular electronic device: field-effect transistor with a polythiophene thin film. Appl. Phys. Lett. 49, 1210–1212.

Velthoen, M.E., Nab, S., and Weckhuysen, B.M. (2018). Probing acid sites in solid catalysts with pyridine UV-Vis spectroscopy. Phys. Chem. Chem. Phys. 20, 21647–21659.

Wang, Y., Feng, L., and Wang, S. (2019). Conjugated polymer nanoparticles for imaging, cell activity regulation, and therapy. Adv. Funct. Mater. 29, 1806818.

Wei, Z., He, J., Liang, T., Oh, H., Athas, J., Tong, Z., Wang, C., and Nie, Z. (2013). Autonomous self-healing of poly(acrylic acid) hydrogels induced by the migration of ferric ions. Polym. Chem. 4, 4601–4605. https://doi.org/10.1039/C3PY00692A.

Yang, J., Zhao, Z., Wang, S., Guo, Y., and Liu, Y. (2018). Insight into high-performance conjugated polymers for organic field-effect transistors. Chem 4, 2748–2785. https://doi.org/10.1016/j.chempr.2018.08.005.

Zangoli, M., Di Maria, F., Zucchetti, E., Bossio, C., Antognazza, M., Lanzani, G., Mazzaro, R., Corticelli, F., Baroncini, M., and Barbarella, G. (2017). Engineering thiophene-based nanoparticles to induce phototransduction in live cells under illumination. Nanoscale 9, 9202–9209.

Zhang, Y., Bi, P., Wang, J., Jiang, P., Wu, X., Xue, H., Liu, J., Zhou, X., and Li, Q. (2015). Production of jet and diesel biofuels from renewable lignocellulosic biomass. Appl. Energy 150, 128–137.

Zucchetti, E., Zangoli, M., Bargigia, I., Bossio, C., Di Maria, F., Barbarella, G., D'Andrea, C., Lanzani, G., and Antognazza, M.R. (2017). Poly (3-hexylthiophene) nanoparticles for biophotonics: study of the mutual interaction with living cells. J. Mater. Chem. B 5, 565–574.

STAR+METHODS

KEY RESOURCES TABLE

Reagent or Resource	Source	Identifier
Chemicals and Regents		
Tetrahydrofuran	Sigma Aldrich	109-99-9
Poly(acrylic acid) (MW = 1800 Da)	Sigma Aldrich	9003-01-4
Copper (II) chloride	Sigma Aldrich	7447-39-4
Cobalt (II) chloride hexahydrate	Sigma Aldrich	7791-13-1
Methanol	Sigma Aldrich	67-56-1
Ethanol	Sigma Aldrich	64-17-5
N, N-dimethyl formamide	Sigma Aldrich	68-12-2
Water	High-Q distillation system	model # 103S

RESOURCE AVAILABILITY

Lead contact

Further information and requests for resources and reagents should be directed to and will be fulfilled by the lead contact, Jie He (jie.he@uconn.edu).

Materials availability

This study didn't generate new unique reagents.

Data and code availability

- All data reported in this paper will be shared by the lead contact upon request.
- This paper does not have coding.
- Any additional information required to reanalyze the data reported in this paper is available from the lead contact upon request.

METHOD DETAILS

Synthesis of Py-P3HT NPs by nanoprecipitation

2 mg of Py-P3HT was first dissolved in 10 mL THF and was heated at 75°C for 10 min to afford a transparent orange solution, which was used when the temperature went back to RT. Aqueous PAA solution (10 mL) were prepared with different concentration (2 mg/mL,1 mg/mL, 0.5 mg/mL, 0.1 mg/mL, 0.05 mg/mL, 0.01 mg/mL). Then 0.2 mL THF dissolved with Py-P3HT was slowly added into aqueous PAA solution by a microsyringe (50 mL/min) under strong magnetic stirring (1000 rpm). The obtained Py-P3HT NP aqueous solution (10 mL) was placed in hood overnight to evaporate the residual THF, which was then concentrated into 4 mL by blowing nitrogen gas. Same procedures were followed when ethanol, methanol and dioxane were used as precipitant.

pH titration experiment

The pH meter was calibrated following three-point method before use. 1, 0.1 and 0.01 M NaOH and HCl aqueous solution were prepared with the volumetric flask. Firstly, 2 mL Py-P3HT NP aqueous solution (prepared under 0.05 mg/mL PAA) was added into a glass vial, which was then added trace amount of 1 M NaOH solution to achieve a pH as 12. Different amount of HCl aqueous solution was added to decrease the pH continuously until reaching 2.3. Py-P3HT NP aqueous solution were equilibrated for 5 min at room temperature each time when the pH was changed, then the UV-vis of which was measured.

Growth of metal NPs on Py-P3HT NPs

The growth of gold and silver on Py-P3HT NPs was conducted by following such a procedure: 20 mL aqueous $HAuCl_4$ (1 mg/mL) or $AgNO_3$ (1 mg/mL) solution was added into a quartz vial with 2 mL P3HT NPs solution (0.05 mg/mL) followed by the addition of triethanolamine (0.4 mL) as electron donor. Then the vial was sealed with a rubbery stopper and bubbled with nitrogen gas for 10 min. Afterwards the quartz vial was irradiated with white light (halogen lamp) for 5 min. The unreacted metal precursors were removed by dialysis against water.

Fluorescence quenching experiment

100 mM $CuCl_2$ and $CoCl_2$ aqueous solution was prepared and stored in volumetric flash before experiments. 2 mL Py-P3HT NP dioxane solution was added into a quartz cuvette sealed with cap, the fluorescence spectrum of which was then measured. The emission intensity of P3HT NPs at 575 nm without metal ions was used as the standard to quantitate the efficiency of fluorescence quenching. And 5 mL $CuCl_2$ aqueous solution (100 mM) was added into cuvette and mixed with dioxane, the solution equilibrated at RT for 2 min before testing by fluorescence spectrometer. Then, the $CuCl_2$ aqueous solution (100 mM) was added continuously to reaching the volume same as in Figure 5A. There is always a 2 min interval each time between adding $CuCl_2$ solution and fluorescence testing. In the case of cobalt, 40 mL of $CoCl_2$ aqueous solution was directly added into 2 mL Py-P3HT NP dioxane solution, which was then tested by fluorescence spectrometer after equilibrated at RT for 2 min.

Characterizations

Ultraviolet-visible (UV-vis) absorption spectra were recorded on Cary 60 UV-vis spectrometer (Agilent). Fluorescence spectra were recorded on a Cary Eclipse Fluorescence Spectrometer (Agilent). The UV-vis and fluorescence spectra of all samples were measured by using a quartz cuvette (4 mL). Fourier-transform infrared spectra (FTIR) were recorded on a Bruker FTIR spectrometer (ALPHA Platinum-ATR). Py-P3HT NPs sample for FTIR characterization was prepared by dropping the aqueous Py-P3HT NPs solution (20mL) to the top of glass, which was repeated over times after the solvent was evaporated by dry nitrogen gas flow, the red solid power was then collected from the surface of glass and subject to testing. Dynamic light scattering and Zeta potential was tested on Zetasizer Nano ZS (Malvern Instrument). Hydrodynamic diameter (D_h) of NPs was measured by DLS at scattering angle q of 173°. Transmission electron microscopy (TEM) images were recorded on FEI Tecnai 12 G2 Spirit BioTWIN. Lifetime measurement was conducted at a Mini-tau lifetime spectrometer (Edinburgh Instruments). The TEM sample were prepared by dropping the Py-P3HT NP solution to the TEM gird placed on the top of a filter paper, which stand at room temperature for 1 h to fully evaporate the solvent.

QUANTIFICATION AND STATISTICAL ANALYSIS

The diameters of NPs shown in TEM image were measured by ImageJ and the data in Figure 1J was represented as mean ± SD, which were given by Origin. Except this, our study does not include any other statistical analysis or quantification.